

July 24, 2006

Nonmonotonic $d_{x^2-y^2}$ superconducting gap in electron-doped $\text{Pr}_{0.89}\text{LaCe}_{0.11}\text{CuO}_4$: Evidence of coexisting antiferromagnetism and superconductivity?

Tanmoy Das
Northeastern University

R. S. Markiewicz
Northeastern University

A. Bansil
Northeastern University

Recommended Citation

Das, Tanmoy; Markiewicz, R. S.; and Bansil, A., "Nonmonotonic $d_{x^2-y^2}$ superconducting gap in electron-doped $\text{Pr}_{0.89}\text{LaCe}_{0.11}\text{CuO}_4$: Evidence of coexisting antiferromagnetism and superconductivity?" (2006). *Physics Faculty Publications*. Paper 405. <http://hdl.handle.net/2047/d20004182>

Nonmonotonic $d_{x^2-y^2}$ superconducting gap in electron-doped $\text{Pr}_{0.89}\text{LaCe}_{0.11}\text{CuO}_4$: Evidence of coexisting antiferromagnetism and superconductivity?

Tanmoy Das, R. S. Markiewicz, and A. Bansil

Physics Department, Northeastern University, Boston, Massachusetts 02115, USA

(Received 31 March 2006; revised manuscript received 25 June 2006; published 24 July 2006)

Recent experiments on $\text{Pr}_{0.89}\text{LaCe}_{0.11}\text{CuO}_4$ observe an anisotropic spin-correlation gap and a nonmonotonic superconducting (SC) gap, which we analyze within the framework of a t - t' - t'' - t''' - t^{iv} - U model with a $d_{x^2-y^2}$ pairing interaction including a third-harmonic contribution. By introducing a realistic broadening of the quasiparticle spectrum to reflect small-angle scattering, our computations explain the experimental observations, especially the presence of a maximum in the leading-edge gap in the vicinity of the hot spots. Our analysis suggests that the material behaves like a two-band superconductor with the d -wave third harmonic acting as the interband pairing gap, and that the antiferromagnetic and SC orders coexist in a uniform phase.

DOI: 10.1103/PhysRevB.74.020506

PACS number(s): 74.72.Dn, 74.20.Rp, 74.25.Dw, 74.25.Jb

Recent Raman scattering¹ and angle-resolved photoemission spectroscopy (ARPES) experiments² on electron-doped $\text{Pr}_{0.89}\text{LaCe}_{0.11}\text{CuO}_4$ (PLCCO) find a $d_{x^2-y^2}$ superconducting (DSC) gap, which varies nonmonotonically along the Fermi surface (FS). The gap increases as one moves away from the nodal direction toward the hot-spot region in the Brillouin zone (BZ) where it attains a maximum value. It then decreases as one approaches the zone boundary along the antinodal direction. The involvement of the hot spots suggests that the bosonic pairing possesses a magnetic origin.^{3,4} If we assume that the system continues to remain uniform with doping, and recall that the residual gap in a half-filled antiferromagnetic (AFM) insulator yields two FS pockets on electron doping, these observations present a striking conundrum: The leading-edge gap is the largest in the momentum region of the hot spots where there are no segments of the FS and quasiparticle states lie well below the Fermi energy.

In this Rapid Communication, we discuss a relatively simple route for resolving this dilemma and understanding the behavior of the superconducting state of PLCCO. In particular, we consider a uniformly doped system with coexisting AFM and DSC orders, where the quasiparticle spectrum is broadened realistically to reflect the effects of small-angle scattering. We thus obtain in the normal state a finite spectral weight at the Fermi energy (E_F) throughout the BZ, and when a third-harmonic term is included in the pairing interaction, the computed leading-edge gap along the FS reproduces the corresponding experimental variations remarkably well. The third-harmonic contribution possesses the proper symmetry to couple the DSC order parameter on the two FS pockets to induce a maximum in the leading-edge gap around the hot spots even though the hot spots lie outside the momentum region of the two FS pockets. Notably, nonmonotonic gap variations have been obtained in some earlier calculations,³⁻⁵ but we are not aware of a previous study involving a realistic model of electron doping with two FS pockets.

Our study gives insight into the issue of well-known asymmetry between the properties of cuprates with electron vs hole doping, which has been a subject of considerable recent debate (see, e.g., Ref. 6). There is growing evidence that the *normal* state of the electron-doped cuprates can be

described as an AFM metal up to a quantum critical point near optimal doping, and that nanoscale phase separations or stripe physics so prominent in the hole-doped case are weak or absent in the electron-doped systems.^{7,8} Since our analysis based on a single-phase model in which the AFM and DSC orders coexist is able to reasonably explain nonmonotonic gap variations, it supports the scenario that the system remains uniform with electron doping not only in the normal but also in the SC state without the intervention of other orders.

We model PLCCO as a uniformly doped spin density wave (SDW) antiferromagnet with d -wave superconductivity. At the mean-field level, there is long-range AFM order, but when fluctuations are included, the Néel temperature T_N becomes zero (in the absence of interlayer coupling), and the mean-field gap turns into a pseudogap Δ^* with crossover temperature T^* . In the SC doping range the FS consists of a necklace of two types of pockets: an electronlike pocket near the antinodal point $(\pi, 0)$, and a holelike pocket near the $(\pi/2, \pi/2)$ nodal point. A pseudogap near the hot spot separates the two pockets. Our one-band tight-binding (TB) model Hamiltonian with competing AFM and DSC is

$$H = \sum_{\vec{k}, \sigma} \xi_{\vec{k}} c_{\vec{k}, \sigma}^\dagger c_{\vec{k}, \sigma} + U_Q \sum_{\vec{k}, \vec{k}'} c_{\vec{k}+\vec{Q}, \uparrow}^\dagger c_{\vec{k}, \uparrow} c_{\vec{k}', \downarrow}^\dagger c_{\vec{k}', \downarrow} + \sum_{\vec{k}, \vec{k}'} V(\vec{k}, \vec{k}') c_{\vec{k}, \uparrow}^\dagger c_{-\vec{k}, \downarrow}^\dagger c_{-\vec{k}, \downarrow} c_{\vec{k}', \uparrow}, \quad (1)$$

where $c_{\vec{k}, \sigma}^\dagger$ ($c_{\vec{k}, \sigma}$) is the electronic creation (destruction) operator with momentum \vec{k} and spin σ . The independent particle dispersion with respect to the chemical potential E_F is given by^{9,10}

$$\xi_{\vec{k}} = -2t[c_x(a) + c_y(a)] - 4t'c_x(a)c_y(a) - 2t''[c_x(2a) + c_y(2a)] - 4t'''[c_x(2a)c_y(a) + c_y(2a)c_x(a)] - 4t^{iv}c_x(2a)c_y(2a) - E_F, \quad (2)$$

with $c_i(aa) = \cos(a\vec{k}_i \cdot a)$ and a the lattice constant.

The effective on-site AFM repulsion U_Q is taken to be doping dependent.⁷ The AFM gap $U_Q S$ arises from a finite

expectation value of the staggered magnetization S at the commensurate ordering wave vector $\vec{Q}=(\pi, \pi)$. The d -wave superconductivity including first and third harmonics is defined by^{3,11}

$$\begin{aligned}\Delta_{\vec{k}} &= \Delta_{1\vec{k}} + \Delta_{3\vec{k}} = \sum_{\vec{k}'} V(\vec{k}, \vec{k}') \langle c_{\vec{k}', \uparrow}^\dagger c_{-\vec{k}', \downarrow}^\dagger \rangle \\ &= \sum_i \Delta_i g_{i\vec{k}} = \sum_i g_{i\vec{k}} V_i \sum_{\vec{k}'} g_{i\vec{k}'} \langle c_{\vec{k}', \uparrow}^\dagger c_{-\vec{k}', \downarrow}^\dagger \rangle,\end{aligned}\quad (3)$$

with $i=1, 3$ and $g_{i\vec{k}}=[c_x(ia) - c_y(ia)]/2$.

The Hamiltonian of Eq. (1) is diagonalized straightforwardly.¹¹ The resulting quasiparticle dispersion consists of upper (UMB) and lower (LMB) magnetic bands, each gapped via the DSC pairing as

$$E_{\vec{k}}^{U+(L+)} = -E_{\vec{k}}^{U-(L-)} = \sqrt{(\xi_{\vec{k}}^\pm \pm E_{0\vec{k}})^2 + \Delta_{\vec{k}}^2}, \quad (4)$$

where $E_{0\vec{k}}^2 = (\xi_{\vec{k}}^-)^2 + (U_Q S)^2$ and $\xi_{\vec{k}}^\pm = (\xi_{\vec{k}} \pm \xi_{\vec{k}+\vec{Q}})/2$. The SDW magnetization S per site is evaluated self-consistently at each temperature via the equations

$$\begin{aligned}S &= \sum_{\vec{k}} \alpha_{\vec{k}} \beta_{\vec{k}} \{ [(v_{\vec{k}}^-)^2 - (v_{\vec{k}}^+)^2] + [(v_{\vec{k}}^+)^2 - (u_{\vec{k}}^+)^2] f(E_{\vec{k}}^{U+}) \\ &\quad - [(v_{\vec{k}}^-)^2 - (u_{\vec{k}}^-)^2] f(E_{\vec{k}}^{L+}) \},\end{aligned}\quad (5)$$

where $f(E) = 1/[\exp(\beta E) + 1]$ is the Fermi function with $\beta = 1/k_B T$. The expressions for $\alpha_{\vec{k}}$, $\beta_{\vec{k}}$, $u_{\vec{k}}^\pm$, and $v_{\vec{k}}^\pm$ are the same as Eqs. (9) and (14), respectively, of Ref. 11. The self-consistent SC gap equations are

$$\Delta_i = -V_i \sum_{\vec{k}} \Delta_{\vec{k}} g_{i\vec{k}} \left(\frac{\tanh(\beta E_{\vec{k}}^{U+}/2)}{2E_{\vec{k}}^{U+}} + \frac{\tanh(\beta E_{\vec{k}}^{L+}/2)}{2E_{\vec{k}}^{L+}} \right). \quad (6)$$

The one-particle Green's function is

$$\begin{aligned}G(\vec{k}, \omega) &= \frac{[\omega Z + \xi_{\vec{k}}^+ + E_{0\vec{k}}] f(E_{\vec{k}}^{U+})}{(\omega^2 - \Delta_{\vec{k}}^2) Z^2 - (\xi_{\vec{k}}^+ + E_{0\vec{k}})^2} \\ &\quad + \frac{[\omega Z + \xi_{\vec{k}}^+ - E_{0\vec{k}}] f(E_{\vec{k}}^{L+})}{(\omega^2 - \Delta_{\vec{k}}^2) Z^2 - (\xi_{\vec{k}}^+ - E_{0\vec{k}})^2},\end{aligned}\quad (7)$$

where we have included broadening due to small-angle elastic scattering^{12,13} with the associated renormalization factor $Z = 1 + i\Gamma_0(\omega) \text{sgn}(\omega) / \sqrt{\omega^2 - \Delta_{\vec{k}}^2}$. $\Gamma_0(\omega)$ is the normal-state scattering rate, discussed below. The corresponding spectral intensity is $A(\vec{k}, \omega) = -\text{Im}[G(\vec{k}, \omega)] / \pi$.

We fitted the dispersion given by Eq. (4) to the ARPES results² on PLCCO at 30 K to obtain the relevant TB parameters as follows: $t=0.12$ eV, $t'=-0.06$ eV, $t''=0.034$ eV, $t'''=0.007$ eV, $t^{iv}=0.02$ eV, with $E_F=-0.082$ eV at 11% doping.¹⁴ The effective AFM parameter is found to be $U_Q=4.15t$, which yields a self-consistent value of the magnetization S of 0.281 from Eq. (5).

Figure 1 clarifies the nature of the quasiparticle spectrum and the FS. As Eq. (4) shows, the noninteracting band is split via the AFM interaction into upper and lower bands. As seen

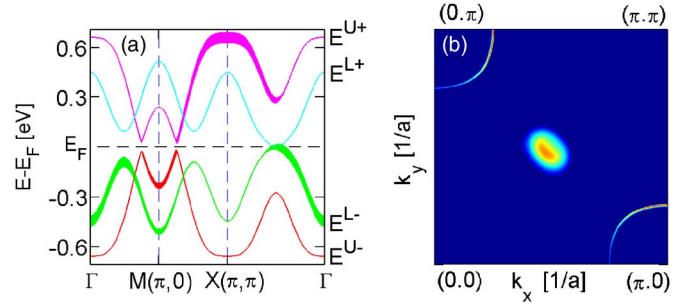


FIG. 1. (Color online) (a) Computed quasiparticle spectrum of PLCCO at 11% doping. Artificially large values of the pairing interaction parameters ($\Delta_1=20$ meV and $\Delta_3=-6$ meV) have been used to highlight the effect of the SC gap, which splits the UMB and the LMB into the pair of bands $E^{U\pm}$ (magenta and red) and $E^{L\pm}$ (cyan and green), respectively. Spectral weight is represented by the vertical width of the bands. (b) FS map in PLCCO at 30 K (normal state) obtained by integrating the spectral intensity of Eq. (7) over a small energy window of ± 5 meV around E_F . High intensity is denoted by red and low by blue.

from Fig. 1(a), each of these bands is further split by the SC interaction to yield pairs of bands $E^{U\pm}$ (magenta and red) and $E^{L\pm}$ (cyan and green), which lie symmetrically above and below E_F . [Note that the SC gap has been made artificially large in Fig. 1(a) to highlight the effect of the SC splitting.] The spectral weights for various bands (proportional to the vertical width of shading) are seen to vary greatly with \mathbf{k} . In effect, the spectral weight of the non-interacting band is redistributed between the UMB and the LMB through the AFM order, and it is modified further via the SC order at very small energy scales of a few meV. Above E_F , we see from Fig. 1(a) that most of the spectral intensity resides in the UMB E^{U+} (magenta) along the $(\pi, 0) \rightarrow (\pi, \pi) \rightarrow (\pi/2, \pi/2)$ line. At other momenta, the spectral weight generally lies below E_F and is carried by the E^{L-} band (green). Figure 1(b) shows a map of the normal state (30 K) FS. This FS is consistent with the experimental results on electron-doped $\text{Nd}_{0.87}\text{Ce}_{0.13}\text{CuO}_4$ (NCCO),^{15,16} and it can be understood with reference to the band structure of Fig. 1(a). The E^{U-} band (red) gives rise to the $(\pi, 0)$ -centered electron pockets, while the $(\pi/2, \pi/2)$ -centered hole pocket arises from the E^{L-} band (green).

Figure 2 gives further insight into the nature of the quasiparticle spectrum and the associated spectral intensity in PLCCO. The computed energy bands in the normal state along the three cuts used in the fitting procedure are compared directly with the corresponding experimental dispersions in Figs. 2(a)–2(c). The overall agreement is seen to be quite good, although a discrepancy is evident in (a) for the antinodal cut in that the computed size of the electron pocket around $(\pi, 0)$ is smaller than that indicated by the experimental data.¹⁷ Notably, due to the presence of the AFM gap, quasiparticle states along the hot spot in (b) lie well below E_F , leading to a suppression of the spectral weight up to binding energies of about 60 meV. In contrast, along the nodal direction in (c), the quasiparticle band crosses E_F , and as already pointed out, gives rise to the $(\pi/2, \pi/2)$ centered hole pockets.

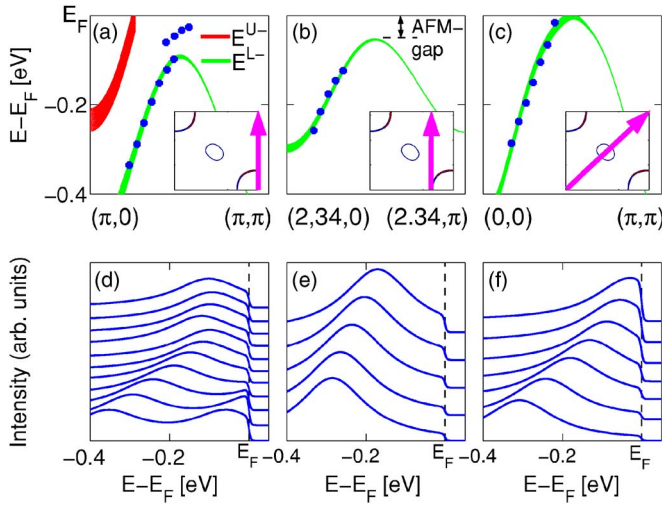


FIG. 2. (Color online) (a)–(c) Quasiparticle spectrum of PLCCO with 11% doping in the normal state at 30 K along three different lines (see insets) in the (k_x, k_y) plane. Spectral weights are proportional to the widths of lines as in Fig. 1(a). Blue dots give the corresponding experimental dispersions taken from Ref. 2. (d)–(f) Spectral intensity obtained from Eq. (7) as a function of binding energy for a series of momenta where the actual momentum values correspond to the experimental points (blue dots) in (a)–(c).

The spectral intensity computed from the imaginary part of the one-particle Green's function of Eq. (7) is shown for a series of momenta in the bottom row of Fig. 2. Here the cuts in the top and bottom sets of panels correspond to each other. For example, in Fig. 2(e) the five spectra shown refer to the five k points given by the blue dots in Fig. 2(b) with the lowest spectrum in (e) corresponding to the leftmost dot in (b). The computations assume a k -independent broadening function of form $\Gamma_0(\omega) = C_0[1 + (\omega/\omega_0)^p]$, which is similar to a form that has been proposed for hole-doped cuprates.¹⁸ Parameter values of $C_0 = 0.1$ eV, $\omega_0 = 1.59$ eV, with $p = 3/2$ reasonably reproduce the experimentally observed broadenings.¹⁹ We emphasize that, for our purposes, the detailed spectral shape is not so important. The key is the presence of quasiparticle broadening, which allows the development of a finite spectral weight at E_F and the formation of the leading-edge superconducting gap at all momenta, even though the underlying quasiparticle states lie well below the E_F at most momenta.

Figure 3 compares spectral intensities in the vicinity of the E_F in the normal and the SC state at four different momenta A – D (see insets). We see that in Figs. 3(a)–3(c) the midpoint of the leading edge of the 8 K spectrum (solid lines) is shifted by Δ_{shift} toward higher binding energies with respect to the spectrum at 30 K (dashed lines), while along the nodal direction in Fig. 3(d), this shift vanishes due to the node in the d -wave gap. Experiments² find a leading-edge gap Δ_{shift} of 2.0 meV along the antinodal direction at the momentum point A ($\pi, 0.8$), which increases to 2.5 meV at the hot spot B ($2.34, 1.0$); Δ_{shift} then decreases to 1.6 meV at C ($1.85, 1.23$) and becomes zero along the nodal direction at the point D ($1.52, 1.52$). The computations of Fig. 3 reproduce this behavior. For this purpose, the superconducting parameters are found to be $V_1 = -76$ meV and $V_3 = 54$ meV,

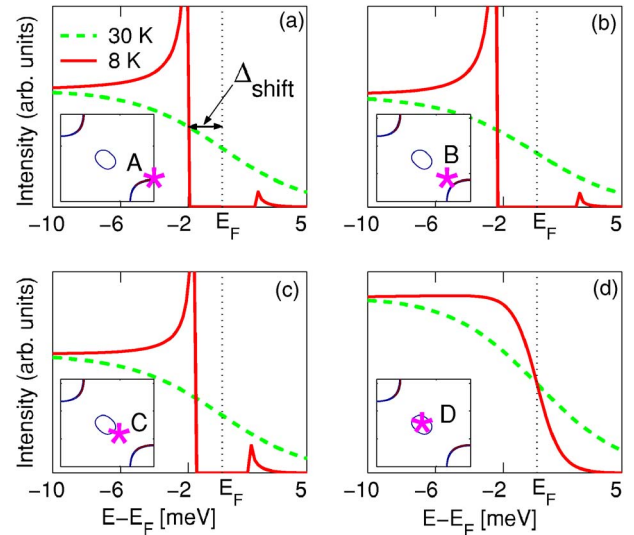


FIG. 3. (Color online) Spectral intensity computed from Eq. (7) in the SC state at 8 K (solid lines) is compared with that for the normal state at 30 K (dashed lines) at four representative momentum points A – D (indicated by stars in the insets). Vertical dotted lines mark E_F , which corresponds to the energy where the normal-state spectral weight falls to half of its value at higher energy. The shift (Δ_{shift}) of the spectral intensity away from the E_F as a leading-edge gap opens up in the SC state is seen in (a)–(c), while this shift vanishes in (d) along the nodal direction due to the d -wave symmetry of the gap.

leading to self-consistent values of the gap parameters at 8 K of $\Delta_1 = 2.50$ meV and $\Delta_3 = -1.1$ meV from Eqs. (3) and (6). We find the electron-boson coupling constants $\lambda_1 = 0.76$ and $\lambda_3 = 0.54$, where $\lambda_i = |V_i|N(0)/2$ and $N(0)$ is the normal-state density of states at E_F . These parameter values yield $T_c = 15$ K, which is in reasonable accord with the experimental value of 26 K. Our calculated T_c gives a value of $2\Delta_1/k_B T_c = 3.9$ close to the BCS value of 3.53. Note that a leading-edge gap is clearly seen near the hot spot in Fig. 3(b). This gap is a direct consequence of the broadening of the spectrum due to small-angle scattering and the associated residual spectral weight at E_F , even though this spectral weight is quite small due to the presence of a sizable pseudogap in the spectrum.

Figure 4(a) shows variations in the leading-edge shift Δ_{shift} and its nonmonotonic and anisotropic nature more clearly. Here the minimum computed value of Δ_{shift} (blue line) is plotted along various directions given by the angle ϕ , where $\phi = 0$ refers to the antinodal direction and $\phi = 45^\circ$ to the nodal direction. The actual momentum points at which the computed values of Δ_{shift} are plotted, shown in the inset, lie close to the noninteracting FS. The corresponding experimental values (red dots) are in good accord with the theoretical results. In particular, the gap reaches a maximum value of about 2.5 meV around $\phi = 18^\circ$ near the hot spot in both theory and experiment. The monotonic d -wave gap obtained by setting $\Delta_3 = 0$ in the calculations is also shown for reference (dashed line) to highlight the nonmonotonic gap variations in the present case.

Our explanation of nonmonotonic gap variations should be distinguished sharply from the notion that one simply

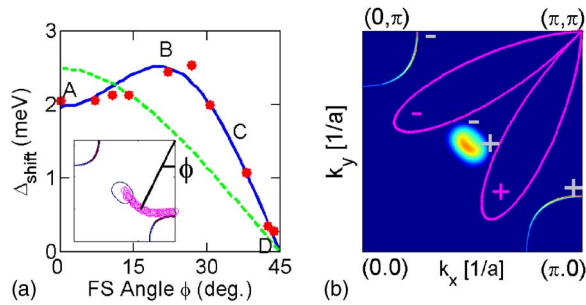


FIG. 4. (Color online) (a) Computed leading-edge gap (blue line) Δ_{shift} at 8 K as a function of the FS angle ϕ is compared with the corresponding experimental results (red dots) on PLCCO (Ref. 2). $A-D$ are momentum points discussed previously in connection with Fig. 3. Green line gives the monotonic gap variation at 8 K in the absence of the third-harmonic term (i.e., $\Delta_3=0$). The inset shows (open circles) the actual momentum points for various directions ϕ where the computed gap values are plotted. (b) Form of the third-harmonic contribution $\Delta_{3\vec{k}}$ (magenta curve) to the gap [see Eq. (3)] is shown schematically on top of the FS map of Fig. 1(b).

observes two different gaps in the experiments, i.e., a SC gap along the pockets and an AFM gap near the hotspots. This alternative picture suffers from the problem that the AFM gap in the normal state of the cuprates is far too large, and, moreover, it is not clear how the leading-edge gap comes about since there are no states at E_F away from the region of the two small FS pockets. Interestingly, the two-band model study of Ref. 20 would require an anomalously small value of t to fit the experimental gap values in PLCCO.

Third-harmonic gaps have been found not only in electron-doped PLCCO (Ref. 2) and NCCO,¹ but also in hole-doped (underdoped) $\text{Bi}_2\text{Sr}_2\text{Ca}_{n-1}\text{Cu}_n\text{O}_{2n+4}$ ($n=1-3$).^{21,22} Interestingly, the third-harmonic contribution in electron-doped cuprates possesses the opposite sign and its size is substantially larger than in the hole-doped case, leading to the non-

monotonic gap variations discussed above. Our study provides insight into this behavior. Separate electron and hole pockets in PLCCO and NCCO are suggestive of two-band²³ superconductivity as in the case of MgB_2 where interband pairing greatly enhances the T_c .²⁴ However, the form of our Hamiltonian in Eq. (1) does not involve a separate interband pairing gap. Figure 4(b) shows that $\Delta_{3\vec{k}}$ possesses the correct symmetry and that its size is maximal in the interval between the two pockets just like the leading-edge gap Δ_{shift} . With this in mind, we propose that the third-harmonic gap $\Delta_{3\vec{k}}$ can be looked upon as playing the role of the interband pairing gap in PLCCO and NCCO. In fact, the hot spot between the two pockets is associated with strong AFM fluctuations in a quasi-two-dimensional system,^{4,12} which in turn are responsible for coupling the UMB and the LMB, and thus coupling the phase of the order parameter on the two FS segments.

The fact that the nonmonotonic gap in our model is intimately associated with the AFM pseudogap indicates that superconductivity arises in an AFM background. These results support the picture of electron-doped cuprates being uniformly doped AFM metals, even in the superconducting state, rather than being phase-separated AFM and SC domains. Note, however, that when fluctuations are added, the present AFM gap becomes a short-range order pseudogap, with a possible Néel-ordering transition at lower temperatures due to interlayer coupling. Open questions remain as to whether superconductivity coexists with this residual three-dimensional (3D) Néel order, or whether the onset of superconductivity destroys either the 3D order, or even the 2D ($T=0$ K) long-range AFM order.

We thank Hong Ding for sharing some of his unpublished results with us. This work is supported by the U.S. DOE Contract No. DE-AC03-76SF00098 and has benefited from the allocation of supercomputer time at NERSC and Northeastern University's Advanced Scientific Computation Center (ASCC).

¹G. Blumberg *et al.*, Phys. Rev. Lett. **88**, 107002 (2002).

²H. Matsui *et al.*, Phys. Rev. Lett. **95**, 017003 (2005).

³F. Guinea, R. S. Markiewicz, and M. A. H. Vozmediano, Phys. Rev. B **69**, 054509 (2004).

⁴V. A. Khodel *et al.*, Phys. Rev. B **69**, 144501 (2004).

⁵H. Yoshimura and D. S. Hirashima, J. Phys. Soc. Jpn. **73**, 2057 (2004); **74**, 712 (2005).

⁶M. Aichhorn *et al.*, cond-mat/0511460 (unpublished).

⁷C. Kusko *et al.*, Phys. Rev. B **66**, 140513(R) (2002).

⁸Y. Dagan *et al.*, Phys. Rev. Lett. **92**, 167001 (2004); Europhys. Lett. **70**, 225 (2005).

⁹R. S. Markiewicz *et al.*, Phys. Rev. B **72**, 054519 (2005).

¹⁰In analogy with NCCO, we expect interlayer coupling effects to be small in PLCCO; see Ref. 9.

¹¹Z. Nazario and D. I. Santiago, Phys. Rev. B **70**, 144513 (2004).

¹²R. S. Markiewicz, Phys. Rev. B **69**, 214517 (2004).

¹³T. Dahm *et al.*, Phys. Rev. B **71**, 212501 (2005).

¹⁴We fitted the experimental dispersions along three different directions given in Figs. 2(d)–2(f) of Ref. 2. Band parameters are comparable to those of NCCO except for a smaller value of t .

¹⁵N. P. Armitage *et al.*, Phys. Rev. Lett. **88**, 257001 (2002).

¹⁶H. Matsui *et al.*, Phys. Rev. Lett. **94**, 047005 (2005).

¹⁷If we attempt to fit a larger electron pocket, we obtain a much larger doping than the 11% value expected for the PLCCO sample used in the experiments of Ref. 2.

¹⁸R. Hlubina and T. M. Rice, Phys. Rev. B **51**, 9253 (1995).

¹⁹A combination of terms linear and quadratic in ω provides an equally good fit.

²⁰Q. Yuan, F. Yuan, and C. S. Ting, Phys. Rev. B **73**, 054501 (2006).

²¹J. Mesot *et al.*, Phys. Rev. Lett. **83**, 840 (1999).

²²H. Matsui *et al.*, Phys. Rev. B **67**, 060501(R) (2003).

²³H. G. Luo and T. Xiang, Phys. Rev. Lett. **94**, 027001 (2005).

²⁴H. Suhl, B. T. Matthias, and L. R. Walker, Phys. Rev. Lett. **3**, 552 (1959).